SCIENCE CHINA
Information Sciences

· Supplementary File ·

Unveiling in-plane and out-of-plane phonon anisotropy in $NbIrTe_4$ through polarization-resolved Raman spectroscopy

Ting WEN[1#], Yalan WANG[2#], Shuang CAI[2#], Ziluo SU[2#], Jiaqi WU[2], Jiaze QIN[2], Chenyin JIAO[2], Zejuan ZHANG[2*], Zenghui WANG[2*] & Shenghai PEI[2*]

[1]School of Electronic Information, Huzhou College, Huzhou 313000, China.
[2]Institute of Fundamental and Frontier Sciences, University of Electronic Science and Technology of China, Chengdu 610054, China.

Appendix A Schematic diagram of the experimental setup

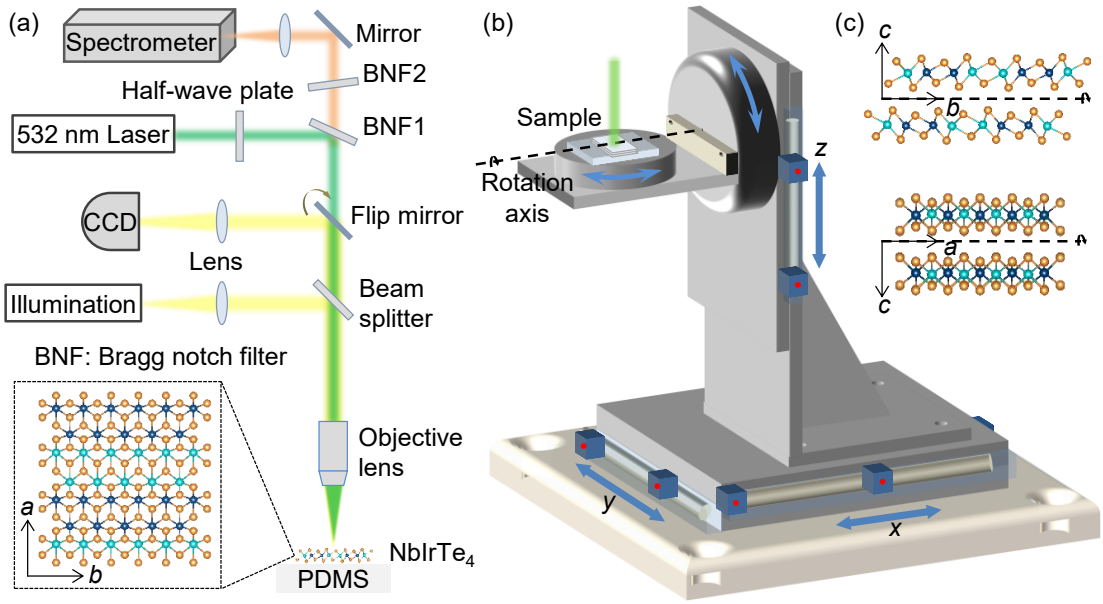

Figure 1 (a) Schematic diagram of the experimental setup; Inset: top view of the crystal structure of $NbIrTe_4$ (in-plane, H). (b) Schematic diagram of the custom-built rotation system. (c) Schematic diagram of the out-of-plane of $NbIrTe_4$.

In our study, $NbIrTe_4$ flakes are mechanically exfoliated and transferred onto poly(dimethylsiloxane) (PDMS). These flakes are then mounted onto a custom-built rotation system (Figure 1(b)), which allows the sample to be continuously rotated from the atomic plane (H, bottom in Figure 1(a)) to the perpendicular planes (V_X and V_Y, Figures 1(c)). By rotating a half-wave plate, the polarization direction of the incident laser (532 nm) is altered, thus enabling determining the crystal orientation of the sample. The *a* and *b* axis of the sample are aligned with the rotation axis

*Corresponding author (email: zejuanzhang@uestc.edu.cn, zenghui.wang@uestc.edu.cn, shpei@uestc.edu.cn)

(Figure 1(b)) to enable Raman detection of the out-of-plane (*ac* and *bc* planes) of $NbIrTe_4$. After mounting the sample, we verify the crystal axis alignment using polarized Raman measurements in H, V_X, and V_Y orientations. The setup (Figure 1(a)) includes a polarized laser focused through a 100× objective, with polarization controlled by a half-wave plate.

Appendix B Schematic diagram and corresponding optical image of the placement configuration of $NbIrTe_4$ on the PDMS substrate

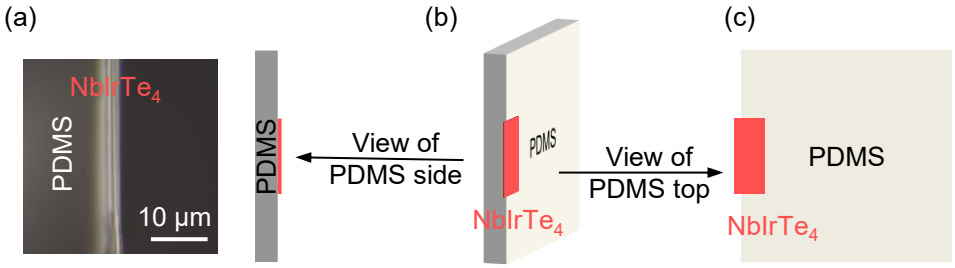

Figure 2 (a) Schematic illustration and corresponding optical image of the placement configuration of $NbIrTe_4$ on the PDMS substrate with view of PDMS side; (b) Three-dimensional schematic of the $NbIrTe_4$/PDMS configuration; (c) Additional schematic illustrating the relative placement of $NbIrTe_4$ on the PDMS substrate with view of PDMS top.

Appendix C Evolution of Raman spectra with sample rotation from in-plane to out-of-plane

We perform angle resolved polarized Raman measurements on $NbIrTe_4$ crystal with sample rotation angle varying from 0° to 90°, *i.e.*, $NbIrTe_4$ crystal gradually rotates from H to V_Y (V_X) orientation as shown in Figure 3(a) (Figure 3(b)). For every sample rotation angle, Raman spectra are measured with polarization parallel ($\theta = 0°$) and perpendicular ($\theta = 90°$) to the crystal X and Z axis. We observe that the process of continuous rotation from H to V is accompanied by the disappearance and appearance of Raman peaks, as well as the variation in peak intensity under the two different polarization directions.

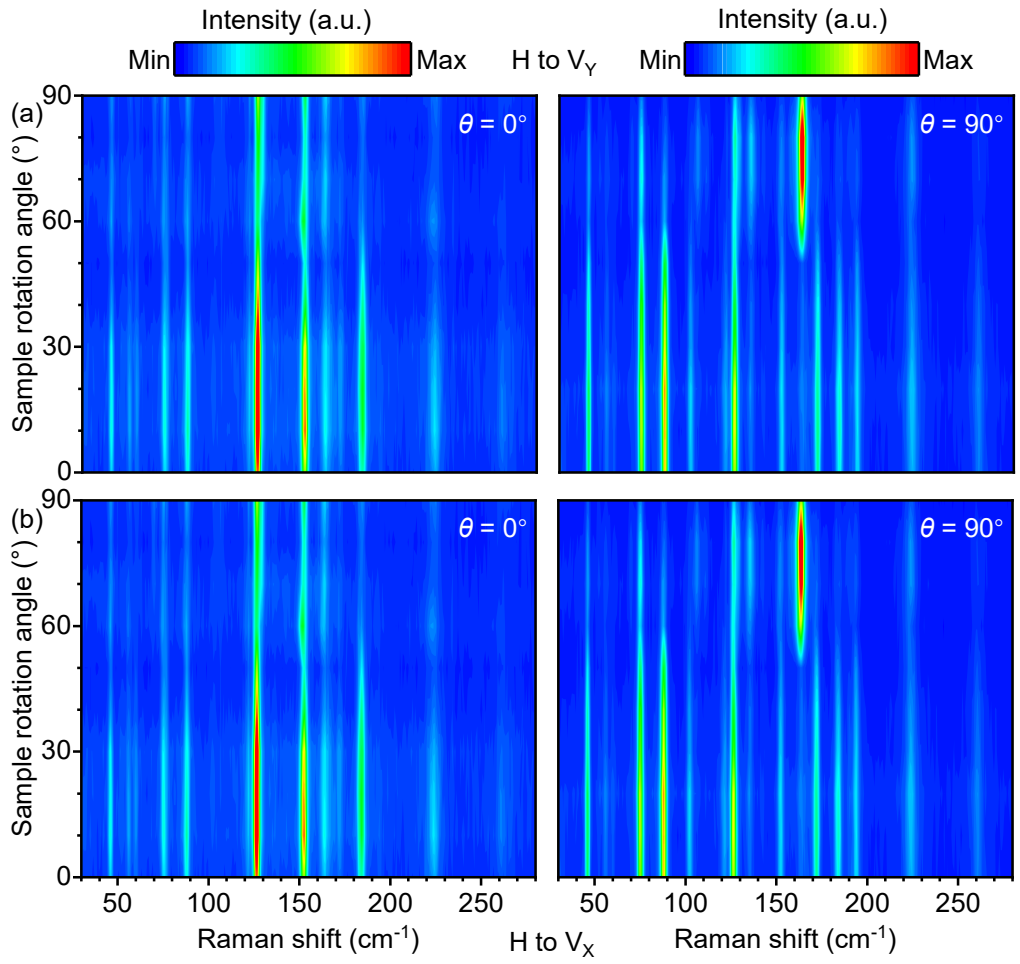

Figure 3 Evolution of Raman spectra with sample rotation from H to (a) V_Y and (b) V_X orientations, with the laser polarization parallel (θ = 0°, left) and perpendicular (θ = 90°, right) to the crystal *c* axis.

Appendix D Polarized Raman measurements of $NbIrTe_4$ crystal on H, V_X and V_Y orientations

Here, we define the θ represents the angle between the laser polarization and the horizontal direction. In the three measurement planes, the $\theta = 0°$ is the laser polarization parallel to Y axis (for H orientation) and the Z axis (for V_X and V_Y orientations).

From the experimental data, through fitting analysis of the Raman peak intensities at different research orientations, we obtain a maximum anisotropy ratio ($R = I_{max}/I_{min}$) of approximately 5.58 under the H orientation (data derived from the A_1^5 Raman mode located at 88.08 cm^{-1}), a maximum anisotropy ratio of about 14.67 under the V_X X (data derived from the A_1^{14} Raman mode located at 163.71 cm^{-1}), and a maximum anisotropy ratio of approximately 25.82 under the V_Y orientation (data derived from the A_1^{14} Raman mode). Our experimental data effectively quantify and reveal the in-plane and out-of-plane optical anisotropy differences of low-symmetric two-dimensional materials.

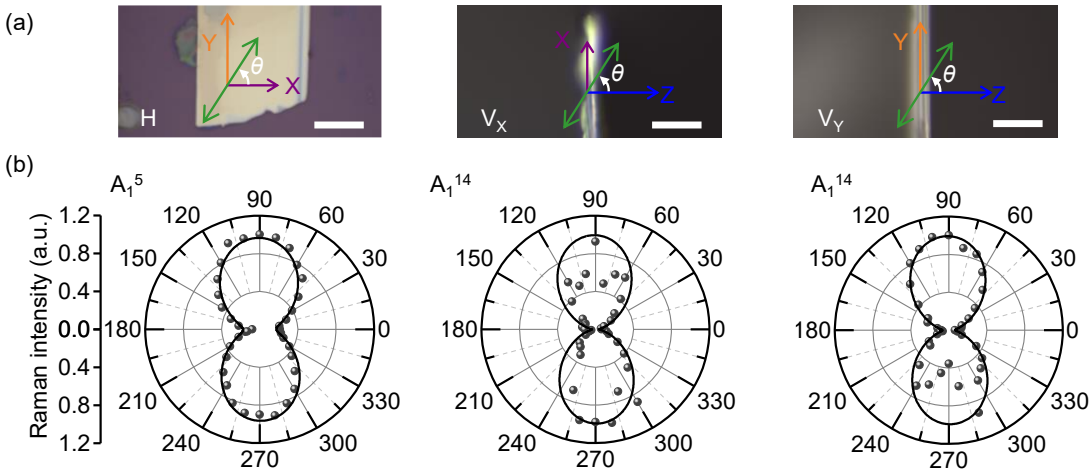

Figure 4 (a) Optical images of the sample under different experimental configurations, scale bar: 10 μm; (b) The polarization plots of Raman peaks with the highest anisotropy ratios at different angles are presented for three distinct experimental configurations. Experimental data (black dots) and fitting results (dashed lines) are shown for comparison. The highest peak value for each mode is normalized.

The observed phenomena can be attributed to the following potential reasons: (1) Crystal symmetry and direction dependence of phonon modes[1,2,3]. In the H and V_X orientations, the angles at which the Raman peaks reach their maximum and minimum intensities are opposite, which could be related to the symmetry of the crystal or the orientation of the phonon modes. In the V_Y orientation, the variation in these angles arises from changes in phonon coupling or scattering mechanisms along different directions. (2) Exciton-phonon interactions[4]. $NbIrTe_4$, as a material with a complex electronic structure, may exhibit strong exciton-phonon interactions. The behavior of excitons could be influenced by the direction of the light field and crystal field in different experimental configurations, which in turn affects the Raman activity. Particularly, the coupling strength and nature of the excitons may differ under various experimental orientations, leading to changes in the anisotropic behavior observed in the Raman spectra. (3) Interlayer coupling and surface effects[5,6]. The laser interacts with different surface structures depending on the experimental configuration. In some configurations, the out-of-plane Raman signals may be enhanced or suppressed due to surface or interface effects, which leads to changes in the anisotropic behavior at specific angles.

Appendix E The anisotropy ratios of different materials

Table 1 The anisotropy ratios of different materials.

	Sample	Orientation	Anisotropy ratios	Ref.
1	BP	In-plane	2.56	4
1	ReS_2	In-plane	4.96	3
1	WTe_2	In-plane	4.95	19
2	$TaIrTe_4$	In-plane	2.5	20
3	$NbIrTe_4$	In-plane	5.58	This work
4	$NbIrTe_4$	Out-of-plane	25.82	

Appendix F Summary table of all the A_1 Raman active modes in $NbIrTe_4$ crystal

Table 2 Summary table of all the A_1 Raman active modes in $NbIrTe_4$ crystal; The peaks highlighted in red are active only under the V_X orientation, while those marked in blue are detectable exclusively under the V_Y orientation.

	A_1 modes						
	Raman shift (cm^{-1})	H-YY (b^2)	H-XX (a^2)	V_X-XX (a^2)	V_X-ZZ (c^2)	V_Y-YY (b^2)	V_Y-ZZ (c^2)
		Area	Area	Area	Area	Area	Area
1	46.09	678.66	230.09	119.07	1156.4	240.86	133.93
2	51.76					54.20	
3	56.15	195.23	116.14	63.21	320.40	141.19	168.43
4	75.12	1352.41	327.45	180.07	2738.06	593.1	219.51
5	88.08	1699.10	335.91	128.51	3311.17	271.58	221.24
6	102.43	394.28			707.84		
7	106.50					300.58	
8	111.26					82.57	
9	121.59	268.56	157.74		447.51		
10	125.94			478.80	171.20		
11	135.53	216.69		156.95	551.15	548.72	
12	142.57	73.89		90.46	126.58	63.59	
13	152.54	599.93	1143.49	599.62	1336.37	221.38	688.60
14	163.71	274.83	309.36	901.86	523.56	3107.74	217.30
15	172.31	840.80	203.64		1449.5	81.80	
16	190.35	100.21				164.38	
17	194.23	580.92			1395.34	121.88	
18	224.31	806.16	553.51	503.99	1770.22	770.97	362.78
19	262.12	499.78	362.87	199.42	1127.76	215.04	197.28

Appendix G Summary table of all the A_2 Raman active modes in $NbIrTe_4$ crystal

Table 3 Summary table of all the A_2 Raman active modes in $NbIrTe_4$ crystal.

A_2 modes			
	Raman shift (cm^{-1})	**H-XY (d^2)** Area	**H-YX (d^2)** Area
1	52.14	53.51	46.0233
2	60.09	57.86	75.9061
3	126.64	1004.71	1256.54
4	184.21	499.79	601.267

Appendix H Summary table of all the B_1 Raman active modes in $NbIrTe_4$ crystal

Table 4 Summary table of all the B_1 Raman active modes in $NbIrTe_4$ crystal. The peaks highlighted in blue are active only under the V_X-XZ sample orientation, while those marked in red are detectable exclusively under the V_X-ZX sample orientation.

B_1 modes			
	Raman shift (cm^{-1})	**V_X-XZ (e^2)** Area	**V_X-ZX (e^2)** Area
1	59.14		53.18
2	74.26		331.85
3	87.10		363.41
4	104.57	182.71	
5	124.97	930.96	934.95
6	171.40		139.07
7	182.22	481.97	363.07

Appendix I Summary table of all the B_2 Raman active modes in $NbIrTe_4$ crystal

Table 5 Summary table of all the B_2 Raman active modes in $NbIrTe_4$ crystal.

B_2 modes			
	Raman shift (cm^{-1})	**V_Y-YZ (f^2)** Area	**V_Y-ZY (f^2)** Area
1	70.23	134.23	135.51
2	127.26	1592.35	1524.7
3	164.23	241.58	304.70
4	184.38	296.53	256.81

Appendix J Raman intensity calculation

According to the classical Raman selection rule, the intensity I of a Raman-active phonon mode is determined by the Raman tensor (R) and the polarization configurations ($\hat{e}_i$, $\hat{e}_s$):

$$I \propto \left|\hat{e}_s \cdot R \cdot \hat{e}_i\right|^2 .$$

Here, $\hat{e}_i$ and $\hat{e}_s$ are the unit vectors of incident laser polarization and scattering light polarization, respectively.

The full 3×3 tensor of a Raman-active mode in $NbIrTe_4$ is:

$$R(\mathrm{A}_1)=\begin{pmatrix} a & 0 & 0 \\ 0 & b & 0 \\ 0 & 0 & c \end{pmatrix},\ R(\mathrm{A}_2)=\begin{pmatrix} 0 & d & 0 \\ d & 0 & 0 \\ 0 & 0 & 0 \end{pmatrix},$$

$$R(\mathrm{B}_1)=\begin{pmatrix} 0 & 0 & e \\ 0 & 0 & 0 \\ e & 0 & 0 \end{pmatrix},\ R(\mathrm{B}_2)=\begin{pmatrix} 0 & 0 & 0 \\ 0 & 0 & f \\ 0 & f & 0 \end{pmatrix}.$$

For XY plane:

$$\hat{e}_i=\begin{pmatrix} \cos\theta \\ \sin\theta \\ 0 \end{pmatrix},\ \hat{e}_s^{\parallel}=\begin{pmatrix} \cos\theta \\ \sin\theta \\ 0 \end{pmatrix},\ \hat{e}_s^{\perp}=\begin{pmatrix} -\sin\theta \\ \cos\theta \\ 0 \end{pmatrix}.$$

For XZ plane:

$$\hat{e}_i=\begin{pmatrix} \cos\theta \\ 0 \\ \sin\theta \end{pmatrix},\ \hat{e}_s^{\parallel}=\begin{pmatrix} \cos\theta \\ 0 \\ \sin\theta \end{pmatrix},\ \hat{e}_s^{\perp}=\begin{pmatrix} -\sin\theta \\ 0 \\ \cos\theta \end{pmatrix}.$$

For YZ plane:

$$\hat{e}_i = \begin{pmatrix} 0 \\ \cos\theta \\ \sin\theta \end{pmatrix},\ \hat{e}_s^{\parallel} = \begin{pmatrix} 0 \\ \cos\theta \\ \sin\theta \end{pmatrix},\ \hat{e}_s^{\perp} = \begin{pmatrix} 0 \\ -\sin\theta \\ \cos\theta \end{pmatrix}.$$

For H (The XY plane)

The 2×2 tensor in the XY plane of $NbIrTe_4$ is:

$$R(\mathrm{A}_1) = \begin{pmatrix} a & 0 \\ 0 & b \end{pmatrix},\ R(\mathrm{A}_2) = \begin{pmatrix} 0 & d \\ d & 0 \end{pmatrix},\ R(\mathrm{B}_1) = 0,\ R(\mathrm{B}_2) = 0.$$

H_XX ($\theta = 0°$, $\hat{e}_i \,//\, \hat{e}_s$):

In this case, $\hat{e}_i = \hat{e}_s = \hat{x} = (1, 0)$, the calculated result of Raman intensity for is:

$$I(\mathrm{A}_1) \propto \left| \begin{pmatrix} 1 & 0 \end{pmatrix} \cdot \begin{pmatrix} a & 0 \\ 0 & b \end{pmatrix} \cdot \begin{pmatrix} 1 \\ 0 \end{pmatrix} \right|^2 = a^2;$$

$$I(\mathrm{A}_2) \propto \left| \begin{pmatrix} 1 & 0 \end{pmatrix} \cdot \begin{pmatrix} 0 & d \\ d & 0 \end{pmatrix} \cdot \begin{pmatrix} 1 \\ 0 \end{pmatrix} \right|^2 = 0;$$

$$I(\mathrm{B}_1) = 0;\ I(\mathrm{B}_2) = 0.$$

H_XY ($\theta = 0°$, $\hat{e}_i \perp \hat{e}_s$):

In this case, $\hat{e}_i = \hat{x} = (1, 0)$, $\hat{e}_s = \hat{y} = (0, 1)$, the calculated result of Raman intensity is:

$$I(\mathrm{A}_1) \propto \left| \begin{pmatrix} 1 & 0 \end{pmatrix} \cdot \begin{pmatrix} a & 0 \\ 0 & b \end{pmatrix} \cdot \begin{pmatrix} 0 \\ 1 \end{pmatrix} \right|^2 = 0;$$

$$I(\mathrm{A}_2) \propto \left| \begin{pmatrix} 1 & 0 \end{pmatrix} \cdot \begin{pmatrix} 0 & d \\ d & 0 \end{pmatrix} \cdot \begin{pmatrix} 0 \\ 1 \end{pmatrix} \right|^2 = d^2;$$

$$I(\mathrm{B}_1) = 0;\ I(\mathrm{B}_2) = 0.$$

H_YY ($\theta = 90°$, $\hat{e}_i \,//\, \hat{e}_s$):

In this case, $\hat{e}_i = \hat{e}_s = \hat{y} = (0, 1)$, the calculated result of Raman intensity for is:

$$I(\mathrm{A}_1) \propto \left| \begin{pmatrix} 0 & 1 \end{pmatrix} \cdot \begin{pmatrix} a & 0 \\ 0 & b \end{pmatrix} \cdot \begin{pmatrix} 0 \\ 1 \end{pmatrix} \right|^2 = b^2;$$

$$I(\mathrm{A}_2) \propto \left| \begin{pmatrix} 0 & 1 \end{pmatrix} \cdot \begin{pmatrix} 0 & d \\ d & 0 \end{pmatrix} \cdot \begin{pmatrix} 0 \\ 1 \end{pmatrix} \right|^2 = 0;$$

$$I(\mathrm{B}_1) = 0;\ I(\mathrm{B}_2) = 0.$$

H_YX ($\theta = 90°$, $\hat{e}_i \perp \hat{e}_s$):

In this case, $\hat{e}_i = \hat{y} = (0, 1)$, $\hat{e}_s = \hat{x} = (1, 0)$, the calculated result of Raman intensity is:

$$I(\mathrm{A}_1) \propto \left| \begin{pmatrix} 0 & 1 \end{pmatrix} \cdot \begin{pmatrix} a & 0 \\ 0 & b \end{pmatrix} \cdot \begin{pmatrix} 1 \\ 0 \end{pmatrix} \right|^2 = 0;$$

$$I(\mathrm{A}_2) \propto \left| \begin{pmatrix} 0 & 1 \end{pmatrix} \cdot \begin{pmatrix} 0 & d \\ d & 0 \end{pmatrix} \cdot \begin{pmatrix} 1 \\ 0 \end{pmatrix} \right|^2 = d^2;$$

$$I(\mathrm{B}_1) = 0; \quad I(\mathrm{B}_2) = 0.$$

For V_X (The XZ plane)

The 2×2 tensor in the XZ plane of $NbIrTe_4$ is:

$$R(\mathrm{A}_1) = \begin{pmatrix} c & 0 \\ 0 & a \end{pmatrix}, \quad R(\mathrm{A}_2) = 0, \quad R(\mathrm{B}_1) = \begin{pmatrix} 0 & e \\ e & 0 \end{pmatrix}, \quad R(\mathrm{B}_2) = 0.$$

V_X_ZZ ($\theta = 0°$, $\hat{e}_i // \hat{e}_s$):

In this case, $\hat{e}_i = \hat{e}_s = \hat{z} = (1, 0)$, the calculated result of Raman intensity for is:

$$I(\mathrm{A}_1) \propto \left| \begin{pmatrix} 1 & 0 \end{pmatrix} \cdot \begin{pmatrix} c & 0 \\ 0 & a \end{pmatrix} \cdot \begin{pmatrix} 1 \\ 0 \end{pmatrix} \right|^2 = c^2;$$

$$I(\mathrm{A}_2) = 0;$$

$$I(\mathrm{B}_1) \propto \left| \begin{pmatrix} 1 & 0 \end{pmatrix} \cdot \begin{pmatrix} 0 & e \\ e & 0 \end{pmatrix} \cdot \begin{pmatrix} 1 \\ 0 \end{pmatrix} \right|^2 = 0;$$

$$I(\mathrm{B}_2) = 0.$$

V_X_ZX ($\theta = 0°$, $\hat{e}_i \perp \hat{e}_s$):

In this case, $\hat{e}_i = \hat{z} = (1, 0)$, $\hat{e}_s = \hat{x} = (0, 1)$, the calculated result of Raman intensity is:

$$I(\mathrm{A}_1) \propto \left| \begin{pmatrix} 1 & 0 \end{pmatrix} \cdot \begin{pmatrix} c & 0 \\ 0 & a \end{pmatrix} \cdot \begin{pmatrix} 0 \\ 1 \end{pmatrix} \right|^2 = 0;$$

$$I(\mathrm{A}_2) = 0;$$

$$I(\mathrm{B}_1) \propto \left| \begin{pmatrix} 1 & 0 \end{pmatrix} \cdot \begin{pmatrix} 0 & e \\ e & 0 \end{pmatrix} \cdot \begin{pmatrix} 0 \\ 1 \end{pmatrix} \right|^2 = e^2;$$

$$I(\mathrm{B}_2) = 0.$$

V_X_XX ($\theta = 90°$, $\hat{e}_i // \hat{e}_s$):

In this case, $\hat{e}_i = \hat{e}_s = \hat{x} = (0, 1)$, the calculated result of Raman intensity for is:

$$I(\mathrm{A}_1) \propto \left| \begin{pmatrix} 0 & 1 \end{pmatrix} \cdot \begin{pmatrix} c & 0 \\ 0 & a \end{pmatrix} \cdot \begin{pmatrix} 0 \\ 1 \end{pmatrix} \right|^2 = a^2;$$

$$I(\mathrm{A}_2) = 0;$$

$$I(\mathrm{B}_1) \propto \left| \begin{pmatrix} 0 & 1 \end{pmatrix} \cdot \begin{pmatrix} 0 & e \\ e & 0 \end{pmatrix} \cdot \begin{pmatrix} 0 \\ 1 \end{pmatrix} \right|^2 = 0;$$

$$I(\mathrm{B}_2) = 0.$$

$\mathrm{V_X}$_XZ ($\theta = 90°$, $\hat{e}_i \perp \hat{e}_s$):

In this case, $\hat{e}_i = \hat{x} = (0, 1)$, $\hat{e}_s = \hat{z} = (1, 0)$, the calculated result of Raman intensity is:

$$I(\mathrm{A}_1) \propto \left| \begin{pmatrix} 0 & 1 \end{pmatrix} \cdot \begin{pmatrix} c & 0 \\ 0 & a \end{pmatrix} \cdot \begin{pmatrix} 1 \\ 0 \end{pmatrix} \right|^2 = 0;$$

$$I(\mathrm{A}_2) = 0;$$

$$I(\mathrm{B}_1) \propto \left| \begin{pmatrix} 0 & 1 \end{pmatrix} \cdot \begin{pmatrix} 0 & e \\ e & 0 \end{pmatrix} \cdot \begin{pmatrix} 1 \\ 0 \end{pmatrix} \right|^2 = e^2;$$

$$I(\mathrm{B}_2) = 0.$$

For $\mathrm{V_Y}$ (The YZ plane)

The 2×2 tensor in the *bc* plane of $\mathrm{NbIrTe_4}$ is:

$$R(\mathrm{A}_1) = \begin{pmatrix} c & 0 \\ 0 & b \end{pmatrix}, \; R(\mathrm{A}_2) = 0, \; R(\mathrm{B}_1) = 0, \; R(\mathrm{B}_2) = \begin{pmatrix} 0 & f \\ f & 0 \end{pmatrix}.$$

$\mathrm{V_Y}$_ZZ ($\theta = 0°$, $\hat{e}_i // \hat{e}_s$):

In this case, $\hat{e}_i = \hat{e}_s = \hat{z} = (1, 0)$, the calculated result of Raman intensity for is:

$$I(\mathrm{A}_1) \propto \left| \begin{pmatrix} 1 & 0 \end{pmatrix} \cdot \begin{pmatrix} c & 0 \\ 0 & b \end{pmatrix} \cdot \begin{pmatrix} 1 \\ 0 \end{pmatrix} \right|^2 = c^2;$$

$$I(\mathrm{A}_2) = 0; \; I(\mathrm{B}_1) = 0;$$

$$I(\mathrm{B}_2) \propto \left| \begin{pmatrix} 1 & 0 \end{pmatrix} \cdot \begin{pmatrix} 0 & f \\ f & 0 \end{pmatrix} \cdot \begin{pmatrix} 1 \\ 0 \end{pmatrix} \right|^2 = 0.$$

$\mathrm{V_Y}$_ZY ($\theta = 0°$, $\hat{e}_i \perp \hat{e}_s$):

In this case, $\hat{e}_i = \hat{z} = (1, 0)$, $\hat{e}_s = \hat{y} = (0, 1)$, the calculated result of Raman intensity is:

$$I(\mathrm{A}_1) \propto \left| \begin{pmatrix} 1 & 0 \end{pmatrix} \cdot \begin{pmatrix} c & 0 \\ 0 & b \end{pmatrix} \cdot \begin{pmatrix} 0 \\ 1 \end{pmatrix} \right|^2 = 0;$$

$$I(\mathrm{A}_2)=0;\ \ I(\mathrm{B}_1)=0;$$

$$I(\mathrm{B}_2)\propto\left|\begin{pmatrix}1 & 0\end{pmatrix}\cdot\begin{pmatrix}0 & f\\ f & 0\end{pmatrix}\cdot\begin{pmatrix}0\\ 1\end{pmatrix}\right|^2=f^2\cdot$$

V_Y_YY ($\theta=90°$, $\hat{e}_i // \hat{e}_s$):

In this case, $\hat{e}_i = \hat{e}_s = \hat{y} = (0, 1)$, the calculated result of Raman intensity for is:

$$I(\mathrm{A}_1)\propto\left|\begin{pmatrix}0 & 1\end{pmatrix}\cdot\begin{pmatrix}c & 0\\ 0 & b\end{pmatrix}\cdot\begin{pmatrix}0\\ 1\end{pmatrix}\right|^2=b^2;$$

$$I(\mathrm{A}_2)=0;\ \ I(\mathrm{B}_1)=0;$$

$$I(\mathrm{B}_2)\propto\left|\begin{pmatrix}0 & 1\end{pmatrix}\cdot\begin{pmatrix}0 & f\\ f & 0\end{pmatrix}\cdot\begin{pmatrix}0\\ 1\end{pmatrix}\right|^2=0\cdot$$

V_Y_YZ ($\theta=90°$, $\hat{e}_i \perp \hat{e}_s$):

In this case, $\hat{e}_i = \hat{y} = (0, 1)$, $\hat{e}_s = \hat{z} = (1, 0)$, the calculated result of Raman intensity is:

$$I(\mathrm{A}_1)\propto\left|\begin{pmatrix}0 & 1\end{pmatrix}\cdot\begin{pmatrix}c & 0\\ 0 & b\end{pmatrix}\cdot\begin{pmatrix}1\\ 0\end{pmatrix}\right|^2=0;$$

$$I(\mathrm{A}_2)=0;\ \ I(\mathrm{B}_1)=0;$$

$$I(\mathrm{B}_2)\propto\left|\begin{pmatrix}0 & 1\end{pmatrix}\cdot\begin{pmatrix}0 & f\\ f & 0\end{pmatrix}\cdot\begin{pmatrix}1\\ 0\end{pmatrix}\right|^2=f^2\cdot$$

Summary

The results above are summarized in Table 6. The calculated results of Raman intensity by I proportional to $\left|\hat{e}_s\cdot R\cdot\hat{e}_i\right|^2$.

	H			V_X			V_Y		
	$\vec{e}_i \parallel \vec{e}_s$		$\vec{e}_i \perp \vec{e}_s$	$\vec{e}_i \parallel \vec{e}_s$		$\vec{e}_i \perp \vec{e}_s$	$\vec{e}_i \parallel \vec{e}_s$		$\vec{e}_i \perp \vec{e}_s$
A_1	θ = 0° (H-XX)	θ = 90° (H-YY)	-	θ = 0° (V_X-ZZ)	θ = 90° (V_X-XX)	-	θ = 0° (V_Y-ZZ)	θ = 90° (V_b-YY)	-
	a^2	b^2		c^2	a^2		c^2	b^2	
A_2	-		θ = 0°/90° (H-XY/YX)	-		-	-		-
			d^2						
B_1	-		-	-		θ = 0°/90° (V_X-ZX/XZ)	-		-
						e^2			
B_2	-		-	-		-	-		θ = 0°/90° (V_Y-ZY/YZ)
									f^2

Table 6 shows that these Raman-active modes not only exhibit a selective response at specific experimental orientations but also show intensity dependence on distinct components of the Raman tensor. Specifically, the A_1 mode is exclusively linked to the tensor components *a*, *b*, and *c*; the A_2 mode is solely determined by component *d*; the B_1 mode is governed by component *e*; and the B_2 mode is uniquely associated with component *f*. This orientation-dependent behavior enables precise modulation of Raman scattering intensity through the control of incident and scattered light polarization directions. Thus, we can clearly distinguish and conduct in-depth studies of the material's behavior along different crystallographic directions, while accurately quantifying the variations in the Raman tensor elements under different measurement orientations.

Appendix K The fitted Raman tensor elements of the 6 stable A_1 modes under 3 experimental configurations

Table 7 The fitted values of the Raman tensor elements in 6 stable A_1 modes under 3 experimental configurations. The fitting formulas under different measurement configurations are summarized in Table 6.

The fitted value of the Raman tensor elements for 6 A_1 modes							
	Raman shift (cm^{-1})	H-YY (b^2)	H-XX (a^2)	V_X-XX (a^2)	V_X-ZZ (c^2)	V_Y-YY (b^2)	V_Y-ZZ (c^2)
		Area	Area	Area	Area	Area	Area
1	46.09	28.27	15.46	19.37	34.83	17.98	12.3
4	75.12	42.62	19.92	23.98	50.61	31.17	18.24
5	88.08	45.24	20.17	20.79	58.09	20.15	16.16
13	152.54	26.66	37.49	28.91	31.65	22.99	28.27
18	224.31	31.95	22.51	31.39	38.8	31.21	19.22
19	262.12	23.6	19.11	22.59	29.65	18.41	14.71

We select 6 representative peaks associated with the A_1 phonon mode for fitting analysis based on the following considerations: (1) these peaks span nearly the entire Raman shift range of $NbIrTe_4$, providing comprehensive coverage of its vibrational characteristics; (2) their relatively strong intensities improve the accuracy of spectral fitting and enhance the reliability of the extracted parameters; and (3) their consistent and stable responses across the three experimental configurations (H, V_X, and V_Y) allow for a detailed comparative analysis of the contributions from individual Raman tensor elements. These features make them well-suited for systematically probing the orientation-dependent anisotropic vibrational behavior of $NbIrTe_4$.

Appendix L The fitted values of the normalized Raman element *c*

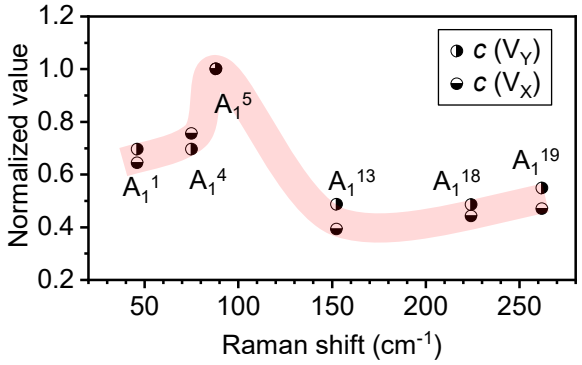

Figure 5 The fitted values of the normalized Raman element *c* varying with the Raman shift in 6 stable A_1 modes under V_X and V_Y orientations; the values are normalized to the maximal value of *c* in each measurement.

A closer comparison of the two extracted *c* values in Figure 5 reveals that they exhibit a consistent variation trend.

Appendix M The results of repeated tests

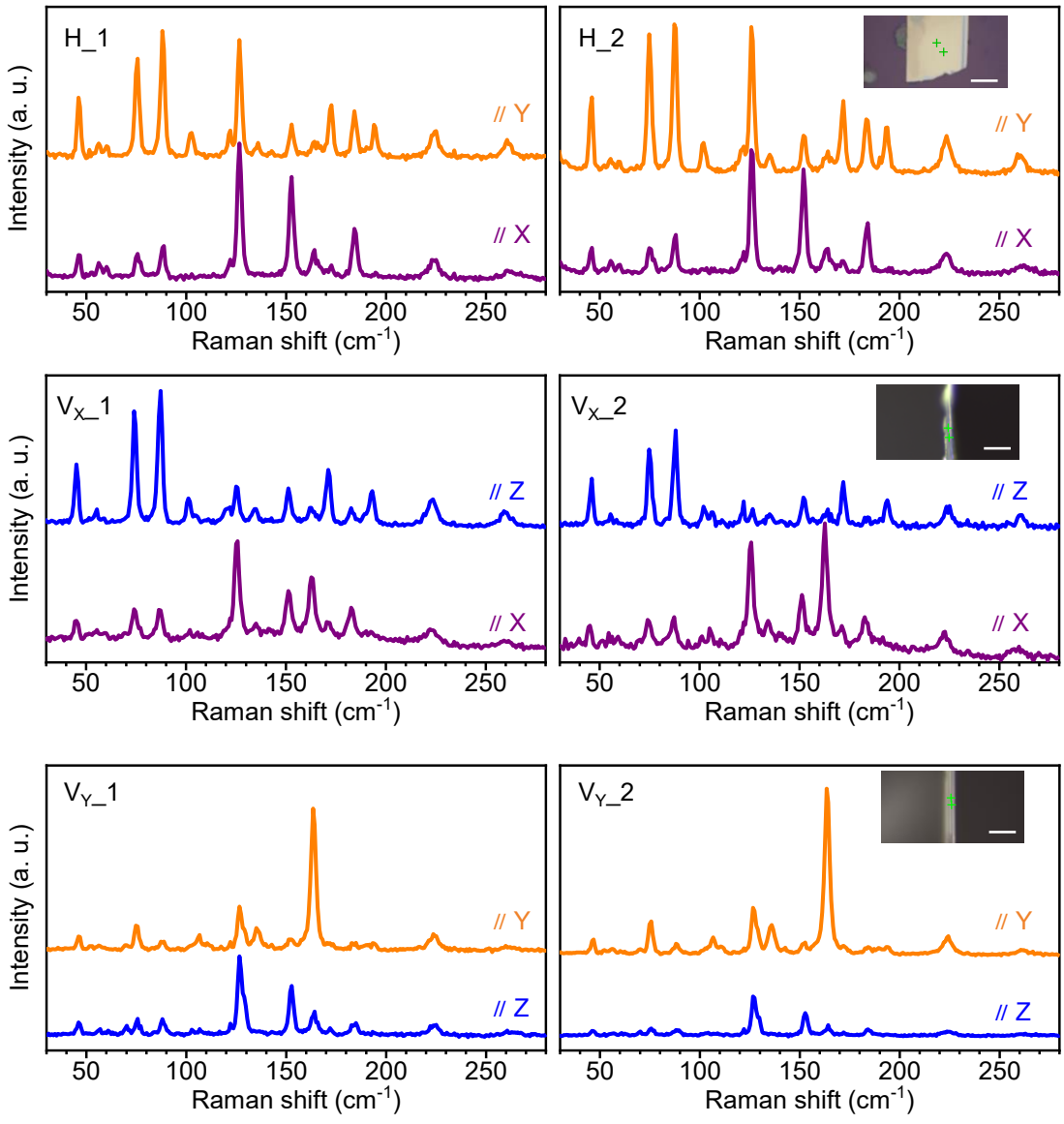

Figure 6 Additional data measured at different sample locations under the three different sample orientations.

Figure 6 shows the Raman spectra measured at different locations on the same sample, exhibiting highly consistent phonon mode positions, intensities, and angular dependencies. These results confirm that the observed phonon behaviors are intrinsic to the material.

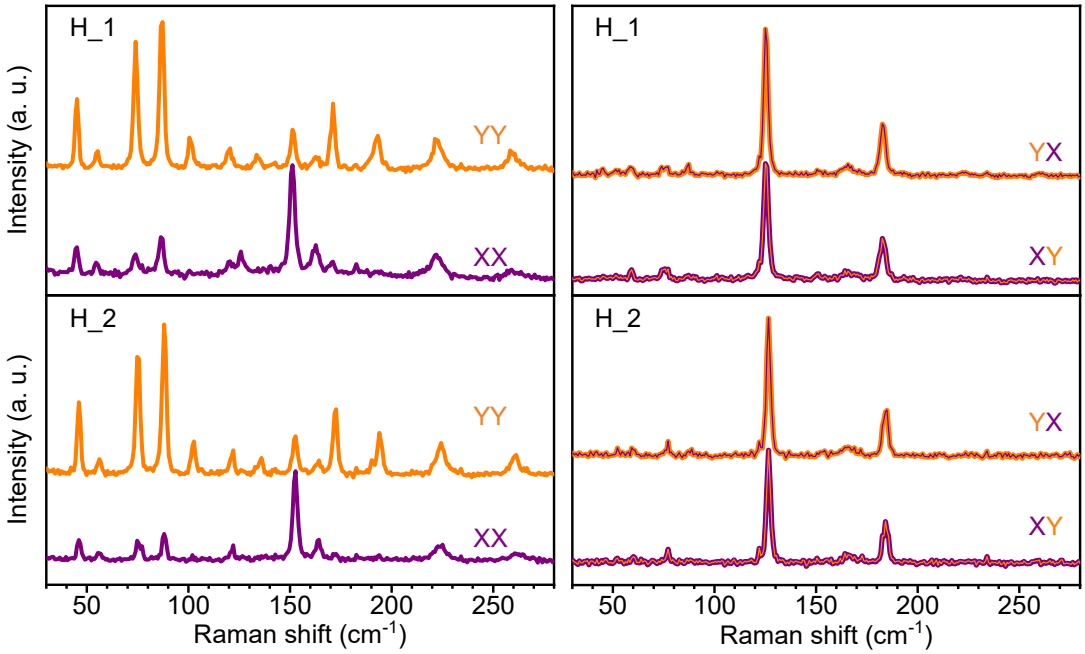

Figure 7 Additional polarization data measured at difference sample locations. the polarization experiment shows good repeatability.

Appendix N Laser information

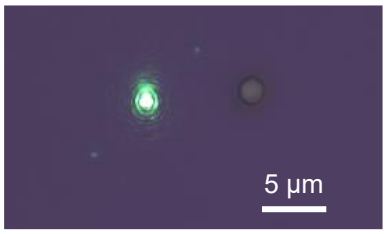

Figure 8 Optical image of the focused laser spot on the Si/SiO_2 substrate using a 100× objective at a laser power of 1 mW; the circular hole next to it has a diameter of 2 μm.

References

1 Huang M, Yan H, Chen C, et al. Phonon softening and crystallographic orientation of strained graphene studied by Raman spectroscopy, Proc Natl Acad Sci USA, 2009, 106: 7304-7308

2 Benshalom N, Asher M, Jouclas R, et al. Phonon-phonon interactions in the polarization dependence of Raman scattering, J Phys Chem C, 2023, 127: 18099-18106

3 Zhang M, Jiao C, Wen T, et al. Discerning the vibrational nature of ReS_2 Raman modes using solid-angle-resolved Raman spectroscopy, Acta Phys Sin, 2022, 71: 140702

4 Empante T A, Zhou Y, Klee V, et al. Chemical vapor deposition growth of few-layer MoTe2 in the 2H, 1T′, and 1T phases: tunable properties of $MoTe_2$ films, ACS Nano, 2017, 11: 900-905

5 Jiao C, Pei S, Wu S, et al. Tuning and exploiting interlayer coupling in two-dimensional van der Waals heterostructures, Rep Prog Phys, 2023, 86: 114503

6 Pei S, Wang Z, Xia J. Interlayer coupling: an additional degree of freedom in two-dimensional materials, ACS Nano, 2022, 16: 11498-11503